Available at www.sciencedirect.com

ScienceDirect

journal homepage: www.elsevier.com/locate/he

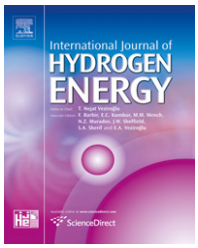

An EIS based study of a Ni–MH battery prototype. Modeling and identification analysis

E.B. Castro [a,*], D.J. Cuscueta [b], R.H. Milocco [c], A.A. Ghilarducci [b], H.R. Salva [b]

[a] Instituto de Investigaciones Fisicoquímicas Teóricas y Aplicadas (INIFTA). Universidad Nacional de La Plata., CCT La Plata-CONICET, Suc 4, CC16 (1900), La Plata, Argentina

[b] Centro Atómico Bariloche – Comisión Nacional de Energía Atómica (CAB-CNEA), Instituto Balseiro – Universidad Nacional de Cuyo (IB-UNCu), CONICET, Av. Bustillo 9500 – CAB (8400) San Carlos de Bariloche, Argentina

[c] Grupo de Control Automático y Sistemas (GCAyS), Depto. Electrotecnia, Facultad de Ingeniería, Universidad Nacional del Comahue, Buenos Aires 1400 (8300) Neuquén, Argentina

ARTICLE INFO

Article history:
Received 30 November 2009
Accepted 17 December 2009
Available online 13 January 2010

Keywords:
Ni–MH battery
Impedance
Modeling
Parameter identification

ABSTRACT

Modeling and simulation of the dynamics of batteries is a useful method to improve design and predict their performance. This paper outlines the development of a simple physicochemical model to simulate the impedance response of the Ni–MH battery system. The model describes the individual electrodes as porous flooded structures where the electrochemical processes take place at the active material/electrolyte interface. The physicochemical system parameters are grouped in such a way that the derived simple model can be experimentally identifiable. Experimental electrochemical impedance spectroscopy (EIS) data, recorded with a laboratory built prototype, are used to identify the model parameters by fitting the theoretical impedance function derived from the model. An analysis of the predicted dependence of the impedance function with the battery SOC and the identifiability of different system parameters are presented.

1. Introduction

The demand for nickel–metal hydride batteries has recently grown for applications ranging from portable electrics to electric and hybrid-electric vehicles. For clean transportation, Ni–MH battery is presently the most promising battery for hybrid-electric vehicles, based on performance and cost. Extensive efforts are being made to develop various advanced nickel–metal hydride batteries to meet commercial requirements.

Traditionally, trial and error experimental testing is a main tool to test and design batteries. However, experiments are time consuming and costly, and experimentally it is difficult to determine the internal processes controlling charge and discharge. Modeling and simulation of batteries is a useful method for battery designers because a good cell model can be used to identify battery mechanisms, determine controlling processes and predict the cell performance. Also the non–destructive evaluation of the state of charge (SOC) of the cell has been the subject of many investigations. EIS measurements have been widely proposed as a tool to provide knowledge of the kinetics of the electrochemical reactions, of the associated charge and mass transport processes, and also as a means to identify structural and physicochemical parameters, several of which may depend on the SOC of the battery [1,6,7,15].

* *Corresponding author*. Tel.: +54 221 425 7430; fax: +54 221 425 7291.
E-mail addresses: bcastro@inifta.unlp.edu.ar (E.B. Castro), cuscueta@cab.cnea.gov.ar (D.J. Cuscueta), milocco@uncoma.edu.ar (R.H. Milocco), friccion@cab.cnea.gov.ar (A.A. Ghilarducci), salva@cab.cnea.gov.ar (H.R. Salva).
0360-3199/$ – see front matter © 2009 Professor T. Nejat Veziroglu. Published by Elsevier Ltd. All rights reserved.
doi:10.1016/j.ijhydene.2009.12.094

The data of sealed commercial cells or batteries are difficult to analyze since the results are generally the combined response of both the positive and the negative electrodes. Several models have been developed ranging from, physicochemical models accounting for the porous nature of the electrode structure and the electrochemical and transport processes in the active materials and in the electrolyte phase Paxtonand Newman, 1997; [5] to equivalent circuit based models of different degree of complexity [4,7,12,16,17].

Although physicochemical models have proved to interpret adequately the dynamics of the battery, the great number of parameters involved makes the parametric identification process almost impossible. On the other hand a low-complexity equivalent circuit modeling is inadequate for interpretation and prediction of the physicochemical processes.

This paper outlines the development of a simple physicochemical model that fits the impedance response of the Ni/MH battery system. The model describes the individual electrodes as flooded porous structures where the electrochemical processes take place at the active material/electrolyte interface. Experimental EIS data recorded with a laboratory built prototype are fitted to the theoretical impedance function derived from the model. An analysis of the predicted dependence of the impedance function with the battery SOC and the identifiability of different system parameters are presented.

2. Experimental

AB5-type alloy with nominal composition of $LmNi_{3.4}Co_{0.3}Mn_{0.3}Al_{0.8}$, where *Lm* (Lanthanum rich mischmetal) is 81% *La*, 13% *Ce*, 2% *Pr* and 4% *Nd*, was mechanically crushed and sieved into particle sizes between 44 and 74 μm. The hydride-forming electrode was prepared with 100 mg of the *Lm*-based alloy powder mixed with equal amount of teflonized carbon black (Vulcan XC-72 with 33 wt% PTFE) as mechanical support, and the mixture was then pressed into a cylindrical matrix under a pressure of 300 MPa at room temperature. The geometric area of the obtained negative electrode was 78.5 mm^2 and the thickness was around 1.7 mm. The anode of the battery was 100 mg of sintered *Co* coated *NiOOH*, with a rectangular shape of 51 mm^2 area and 0.74 mm thickness. The electrodes separator was a glass mat of 0.18 mm thickness and the solution used as electrolyte was *KOH* 8 M.

Fig. 1 shows the laboratory prototype used as battery container. It consists on a stainless steel main body, where the electrodes, the separator and the electrolyte are disposed. The metallic composition of the body and the top piston assure the electrical contact with the battery electrodes.

Electrochemical measurements were carried out at room temperature. The battery activation was guaranteed over 15 electrochemical cycles, by charging the battery with a current of 100 $mAh.g^{-1}$ for 150 min and subsequently discharging them with 100 $mAh.g^{-1}$ up to the cut off potential of −0.6 V. Then the EIS measurements were conducted over a frequency range from 2 mHz to 10 kHz at equilibrium conditions, with a superimposed sinusoidal voltage signal of 6 mV amplitude, using an AUTOLAB PGSTAT30 frequency response analyzer.

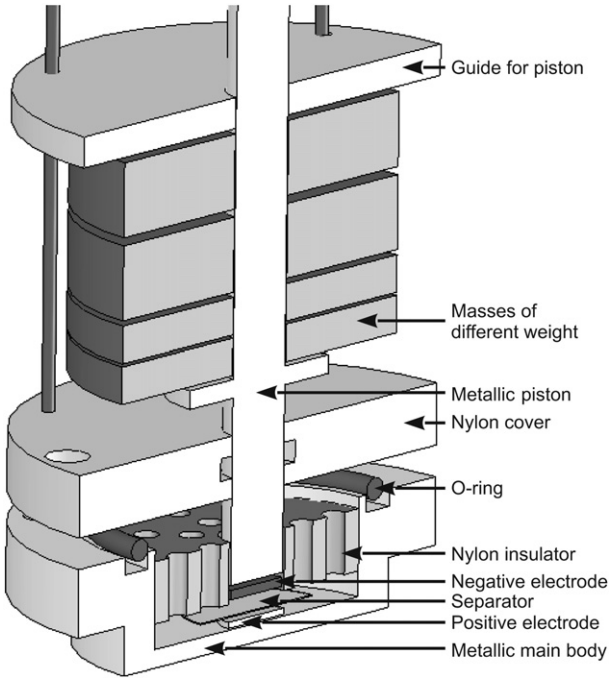

Fig. 1 – Outline of the battery prototype.

3. Theoretical analysis

3.1. Total impedance of the battery

The total impedance function (Z_{BAT}) is derived considering a series connection of the Ni and MH electrodes and the resistive term R_i associated with charge transport in the separator and any other resistive contribution.

$$Z_{BAT}(j\omega) = R_i + Z_{pNI}(j\omega) + Z_{pMH}(j\omega) \quad (1)$$

being Z_{pNi} and Z_{pMH} the impedance functions of the electrodes.

3.2. Impedance of the individual electrodes

Both electrodes are described as porous structures, flooded with a highly concentrated electrolyte (*KOH* 8 M). The charge/discharge processes taking place at the active material/electrolyte interface. In the MH electrode the alloy particles, assumed as spheres of mean radius, constitute the active material and C particles acting as a conducting support [2]. In the Ni electrode the active material is assumed as conformed by spherical *NiOOH* particles, of mean radius, deposited on a conducting support [5].

The impedance function of the porous structure, Z_p may be expressed as [2,9,10]:

$$Z_p\ (j\omega) = \frac{L}{A_p(\kappa+\sigma)}\left[1 + \frac{2 + \left(\frac{\sigma}{\kappa}+\frac{\kappa}{\sigma}\right)\cosh\nu(j\omega)}{\nu(j\omega)\sinh\nu(j\omega)}\right] \quad (2)$$

where

$$\nu(j\omega) = L\left(\frac{\kappa+\sigma}{\kappa\sigma}\right)^{1/2} Z_i^{-1/2}(j\omega)$$

with $j=\sqrt{-1}$, $\omega=2\pi f$, being f the frequency, L the electrode thickness, A_p the corresponding geometric areas (cross section), κ and σ the effective conductivities of the liquid and solid phases respectively and Z_i the impedance of the solid/liquid interface per electrode unit volume ($\Omega\ cm^3$).

As usually $\kappa<<\sigma$, Eq. (2) may be simplified to

$$Z_p(j\omega)=\frac{L}{A_p\kappa}\left[\frac{1}{\nu(j\omega)\tanh\nu(j\omega)}\right]$$
$$\nu(j\omega)=L\left(\frac{1}{\kappa}\right)^{1/2}Z_i^{-1/2}(j\omega) \quad (3)$$

In the following analysis the simplified form of $Z_p(j\omega)$ of Eq. (3) shall be used.

$Z_i(j\omega)$, implies the double layer capacitance impedance, $Z_{dl}(j\omega)$, linked in parallel with the faradaic processes impedance, $Z_F(j\omega)$, i.e.

$$Z_i^{-1}(j\omega)=Z_{dl}^{-1}(j\omega)+Z_F^{-1}(j\omega) \quad (4)$$

where

$$Z_{dl}(j\omega)=\frac{1}{j\omega C_{dl}a_e} \quad (5)$$

being C_{dl} the double layer capacitance per unit interfacial area ($C_{dl}\approx 5\times10^{-5}\ F\ cm^{-2}$) and a_e the interfacial area per unit volume (cm^{-1}).

The faradaic impedance per unit volume ($\Omega\ cm^3$), is given by

$$Z_F(j\omega)=\frac{Z_f(j\omega)}{a_a} \quad (6)$$

where $Z_f(j\omega)$ is the faradaic impedance per unit interfacial area ($\Omega\ cm^2$) and a_a, the active area per unit volume (cm^{-1}).

3.2.1. Derivation of Z_f

The derivation of the faradaic impedance, Z_f, of the Ni and MH electrodes, such as the ones used in the prototype design, is thoroughly described in [2,14,18]. A brief description is given below.

The main processes during discharge at the Ni and MH electrodes are the absorption/desorption of *H* atoms in the active materials, producing the reduction of nickel oxyhydroxide in the positive electrode and the oxidation of the metal hydride in the negative one, an adsorption/absorption reaction mechanism governs the insertion of hydrogen atoms in the hydride forming alloy [11,14,18].

The set of reactions at both electrodes are given as

Ni electrode

$$NiOOH+H_2O+e^-\leftrightarrow Ni(OH)_2+OH^-$$

MH electrode

$$MH_{ad}+OH^-\leftrightarrow H_2O+M+e^-\ (\text{Volmer, adsorption step})$$

$$M+SH_{ab}\leftrightarrow MH_{ad}+S\ (\text{Absorption step})$$

MH_{ad} is an adsorbed hydrogen atom on an active site on the MH alloy surface, SH_{ab} is a hydrogen atom absorbed in an interstitial site in the alloy and S is an empty interstitial site.

The faradaic currents related to these reactions at the Ni and MH electrodes may be expressed as [11,13]

$$i_{Ni}=i^o_{Ni,ref}\left(\frac{x_{sNi}}{x_{refNi}}\exp\left(\frac{\alpha_a F\eta_{Ni}}{RT}\right)-\frac{1-x_{sNi}}{1-x_{refNi}}\exp\left(\frac{\alpha_c F\eta_{Ni}}{RT}\right)\right) \quad (7)$$

$$i_{MH}=i^o_{MH,ref}\left(\frac{x_{sMH}}{x_{refMH}}\frac{(x_{refMH}+K_{eq}(1-x_{refMH}))}{(x_s+K_{eq}(1-x_s))}\exp\left(\frac{\alpha_a F\eta_{MH}(t)}{RT}\right)-\frac{(1-x_{sMH})}{(1-x_{refMH})}\frac{(x_{refMH}+K_{eq}(1-x_{refMH}))}{(x_{sMH}+K_{eq}(1-x_{sMH}))}\exp\left(\frac{\alpha_c F\eta_{MH}(t)}{RT}\right)\right) \quad (8)$$

where:

$x_{sNi}=c_{sNi}/c_{mNi}$, Fractional concentration of hydrogen atoms in the Ni particles at the electrochemical interface.

c_{mNi}, Maximum admissible H concentration in the Ni active material.

$x_{sMH}=c_{sMH}/c_{mNi}$, Fractional concentration of hydrogen atoms in the MH particles at the electrochemical interface.

c_{mMH}, Maximum admissible H concentration in the MH active material

x_{refNi} and x_{refMH}, H fractional concentration in the reference state, $x_{ref}=0.5$

$i^o_{Ni,ref}$, $i^o_{MH,ref}$, Exchange current densities of Ni and MH electrodes at the reference state (SOC = 0.5)

K_{eq}, Equilibrium constant of the absorption step

$\eta_{Ni}=E_{Ni}-E_{eq,MH,ref}$, $\eta_{MH}=E_{MH}-E_{eq,MH,ref}$

E_{Ni}, E_{MH}, Potential at Ni and MH electrochemical interfaces.

$E_{eq,Ni,ref}$, $E_{eq,MH,ref}$, Equilibrium potential of Ni interface and MH interfaces at $x_{ref}=0.5$

The faradic impedance function, $Z_f(j\omega)$, for the Ni and MH electrodes, may be derived, as follows, from equations (7) and (8) after linearization and Fourier transformation:

3.2.1.1. *Ni electrode*.

$$\frac{1}{Z_f(j\omega)}=\frac{\Delta i_{Ni}(j\omega)}{\Delta\eta_{Ni}(j\omega)}=\left(\frac{\partial i_{Ni}}{\partial\eta_{Ni}}\right)_{x_s}+\left(\frac{\partial i_{Ni}}{\partial x_s}\right)_{\eta_1}M(\omega)\frac{\Delta J_H(j\omega)}{\Delta\eta_{Ni}(j\omega)}$$

Being, $M(j\omega)=\Delta x_s(j\omega)/\Delta J_H(j\omega)$ the mass transfer function [8] and J_H the proton flux at active material/electrolyte interface.

Taking into account

$$\Delta J_H(j\omega)/\Delta\eta_{Ni}(j\omega)=\Delta i_{Ni}(j\omega)/(\Delta\eta_{Ni}(j\omega)F)=1/(Z_f(j\omega)F)$$

the faradaic impedance can be written as

$$Z_{fNi}(j\omega)=\left(\frac{\partial i_{Ni}}{\partial\eta_{Ni}}\right)^{-1}_{x_s}\left(1-\left(\frac{\partial i_{Ni}}{\partial x_s}\right)_{\eta_1}\frac{M(j\omega)}{F}\right) \quad (9)$$

The partial derivatives are derived as follows, considering $(\alpha_a-\alpha_c)=1$:

$$\left(\frac{\partial i_{Ni}}{\partial\eta_{Ni}}\right)_{x_s}=\frac{1}{R_{TNi}}=\frac{i^o_{Ni}F}{RT}$$
$$\left(\frac{\partial i_{Ni}}{\partial x_s}\right)_{\eta_1}=\frac{i^o_{Ni}}{x(1-x)} \quad (10)$$

where i^o_{Ni} corresponds to the exchange current density of the Ni electrode, at the corresponding SOC of the EIS measurement.

In the derivation of Eqs. (10), steady state equilibrium has been considered battery equilibrium is assumed as EIS data are recorded at open circuit conditions, so the steady state current, $i_{NI}=0$, accordingly:

$$x = (1 - SOC)_{Ni}$$

$$i^{o}_{Ni} = i^{o}_{Niref} \frac{soc^{\alpha_a}_{Ni}}{\left(1 - soc^{ref}_{Ni}\right)(1 - soc_{Ni})^{\alpha_a - 1}}$$

Introducing eqs. (10) in (9), the final expression for Z_f is

$$Z_{fNi}(j\omega) = R_{TNi} - \frac{RTM_{Ni}(j\omega)}{F^2 soc_{Ni}(1 - soc_{Ni})} \quad (11)$$

The expression for $M(j\omega)$ is derived by solving Fick's laws for the corresponding geometry and boundary conditions.

For the Ni electrode the active material is constituted by spherical Ni oxide particles of mean radius r_{Ni}. The intercalation process takes place at the particle surface/electrolyte interface. Therefore, radial diffusion in a sphere of radius r_{Ni} is considered in the derivation of $M(j\omega)$ [8], with boundary conditions:

$$r = r_{Ni};\ FJ_H = i_{Ni};\ r = 0;\ J_H = 0$$

$$M_{Ni}(j\omega) = \frac{r_{Ni}}{c_{mNi} D_{Ni}} \frac{1}{(1 - \psi_{Ni} coth(\psi_{Ni}))}$$

being

$$\psi_{Ni}(j\omega) = r_{Ni}\sqrt{\frac{j\omega}{D_{Ni}}}$$

where D_{Ni} is the diffusion coefficient of H in the Ni material.

If D_{Ni} is small enough, the mass transfer function, M_{Ni}, may be well represented by a Warburg type function

$$M_{Ni}(j\omega) = -\frac{1}{c_{mNi}\sqrt{D_{Ni} j\omega}}$$

So a simplified form for $Z_{fNi}(j\omega)$ is

$$Z_{fNi}(j\omega) = R_{TNi} + \frac{A_{Ni}}{\sqrt{j\omega}} \quad (12)$$

being

$$R_{TNi} = \frac{RT}{i^{o}_{Ni} F} \text{ and } A_{Ni} = \frac{RT}{F^2 soc_{Ni}(1 - soc_{Ni}) c_{mNi}\sqrt{D_{Ni}}}$$

3.2.1.2. *MH electrode*. $Z_{fMH}(j\omega)$ may be derived from Eq. (8) in an analogous way as $Z_{fNi}(j\omega)$, leading to

$$Z_{fMH}(j\omega) = R_{TMH} + \frac{A_{MH}}{\sqrt{j\omega}} \quad (13)$$

In the derivation of eq. (13), semi infinite diffusion is also assumed (Warburg type diffusion), being

$$R_{TMH} = \frac{RT}{i^{o}_{MH} F}$$

$$A_{MH} = \frac{RT}{F^2 soc_{MH}(1 - soc_{MH}) c_{mMH}\sqrt{D_{MH}}}$$

$$i^{o}_{MH} = i^{o}_{MH,ref}\left(\frac{soc_{MH}}{soc_{refMH}} \frac{\left(soc_{refMH+} K_{eq}(1 - soc_{refMH})\right)}{\left(soc_{MH} + K_{eq}(1 - soc_{MH})\right)} \left(\frac{1 - soc_{MH}}{soc_{MH}}\right)^{\alpha_a}\right)$$

For details see reference [11].

For high values of K_{eq} and $soc_{ref} = 0.5$

$$i^{o}_{MH} = i^{o}_{MH,ref}\left(\left(\frac{1 - soc_{MH}}{soc_{MH}}\right)^{\alpha_a - 1}\right)$$

The complete set of Eqs. (1)–(6), (12), (13) leads to the total impedance of the battery Z_{BAT}.

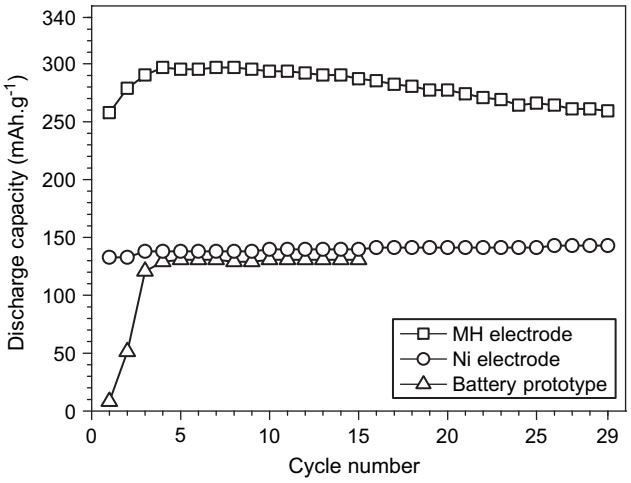

Fig. 2 – Activation and cycling stability of individual electrodes and battery prototype.

3.3. *Parameter identification considerations*

In order to calculate Z_{BAT}, the different parameters of the system must be identified by means of a suitable fitting procedure. An important topic must be analyzed before parametric identification, the theoretical identifiability of the model [3]. The theoretical identifiability implies determining if the model parameters may be identified globally (unique solution), locally (a finite number of solutions) or if they are non-identifiable (infinite number of solutions). The test carried on by using the method proposed in [3] indicates that both electrodes can't be identified individually since the parameters of each can be exchanged giving the same impedance.

On the other hand, according to the different equations of the system, it is impossible the complete identification of the system, as several parameters appear as products. In order to arrive to an expression of Z_{BAT} with identifiable parameters, we shall express Eq. (1) as:

$$Z_{BAT}(j\omega) = R_i + Z_1(j\omega) + Z_2(j\omega) \quad (14)$$

Being:

$$Z_{1,2}(j\omega) = \lambda_{1,2}\left[\frac{1}{v_{1,2}(j\omega)\tanh v_{1,2}(j\omega)}\right] \quad (15)$$

$$\lambda_{1,2} = \frac{L}{A_p k};\ v_{1,2}(j\omega) = \sqrt{j\omega C_{1,2} + \left(\frac{1}{\Re_{1,2} + \frac{\Delta_{1,2}}{\sqrt{j\omega}}}\right)}$$

$$C_{1,2} = \frac{C_{dl} a_e L^2}{\kappa};\ \Re_{1,2} = \frac{R_t \kappa}{L^2 a};\ \Delta_{1,2} = \frac{A\kappa}{L^2 a_a} \quad (16)$$

Now the parameters to be identified are R_i, λ_1, λ_2, C_1, C_2, $\Re_1$, $\Re_2$, Δ_1, Δ_2.

According to the identification analysis, an important consequence of the expression in Eq. (14), is that it is not possible from impedance data only to assign Z_1 or Z_2 to either the Ni or MH electrode. Further on, we shall see how information of the individual electrodes may help in the identification of Z_{MH} and Z_{Ni}.

The structural and physicochemical parameters included in equations (16) i.e. a_a, L, k, R_t, and A, correspond to either a_{aMH}, k_{MH}, R_{tMH}, etc. or a_{aNi}, k_{Ni}, R_{tNi}, etc.

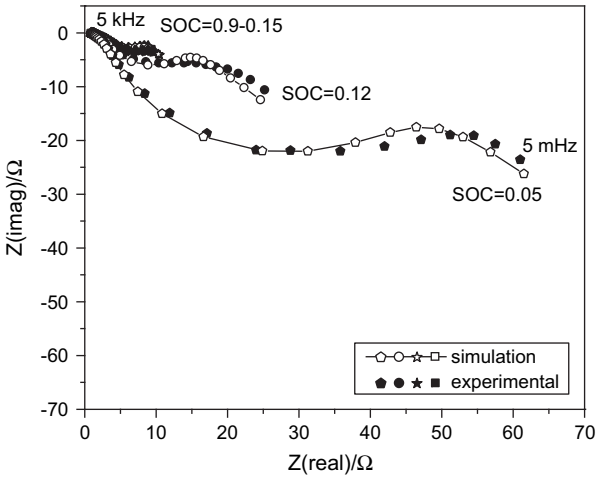

Fig. 3 – Nyquist plots (experimental (•) data and simulation (–○–) results) for 0.05 < SOC < 0.9.

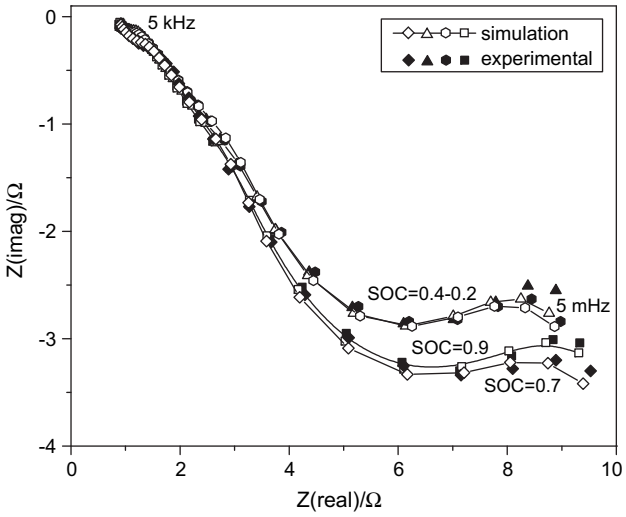

Fig. 4 – Nyquist plots corresponding to 0.2 < SOC < 0.9 (expansion of Fig. 3).

We shall see below how certain physicochemical and structural parameters may be derived after the fitting procedure.

In order to perform the parametric identification, a fitting programme was developed, based on the Nelder-Meade simplex search algorithm included in the Matlab package. The objective function to be minimized was the cost function J_p, defined as

$$J_p = \frac{1}{K}\sum_{k=1}^{K} Ie(p,\omega_k)I^2 = \frac{1}{K}\sum_{k=1}^{K} I\,\frac{Z_e(\omega_k) - Z_P(p,\omega_k)}{Z_e(\omega_k)}I^2$$

where K is the number of experimental frequencies (ω) and $Z_e(\omega k)$ and $Z_P(\omega k)$ the experimental and theoretical impedance values corresponding to the frequency ω_k. This algorithm returns a parameter vector [p] that is a local minimizer of J_p, near the starting vector [p_o], so the whole fitting procedure is highly dependent on the initial values assigned to the [p_o] vector parameters. The fitting was considered acceptable when $J_p < 5.10^{-3}$.

4. Results and discussion

Fig. 2 shows the activation and cycling stability of electrochemical measurements performed in positive and negative electrodes on a laboratory cell. Also it shows the electrochemical discharge capacity of both electrodes and separator in the battery prototype. The maximum discharge capacity reached by the hydride forming alloy is 296.8 mAh.g^{-1} in cycle 4, while the sintered *NiOOH* presents a maximum discharge capacity of 143 mAh.g^{-1}. Accordingly as depicted in Fig. 2, the discharge capacity and state of charge (SOC) of the battery is determined by de *NiOOH* electrode.

4.1. *Experimental EIS data and fitting results*

Fig. 3 depicts, both, Nyquist plots corresponding to experimental EIS data, recorded with the battery prototype at different SOC values, and theoretical EIS data calculated in terms of Eqs. (14–16), using the identified parameters assembled in Table 1.

An expansion corresponding to intermediate SOC values is depicted in Fig. 4. It is interesting to note that no appreciable changes in the battery impedance data can be observed for intermediate SOC values, 0.2 < SOC < 0.9. This same trend has been reported with commercial batteries [1,3,15].

From the expressions given in Eqs. (16), the following relationships may be derived (in the following i = 1,2)

Table 1 – Parameters derived from the fitting procedure.

SOC	R_i/ohm	λ_1	C_1	$\Re_1$	Δ_1	λ_2	C_2	$\Re_2$	Δ_2
0.95	0.84	3.17	4	1.32	<1e-3	2.1	0.06	0.04	0.32
0.85	0.843	3.8	4.85	1.15	<1e-3	2.12	0.022	0.02	0.28
0.72	0.86	2.5	3.4	1.64	<1e-3	5.83	0.036	0.0036	0.077
0.57	0.8	2.74	3.63	1.44	<1e-3	4.9	0.039	0.0034	0.092
0.43	0.84	3.34	4.4	1.1	<1e-3	3.4	0.03	0.0062	0.15
0.29	0.83	2.3	3	1.53	<1e-3	5	0.053	0.0037	0.113
0.15	0.84	2	3.8	1.5	<1e-2	10.7	0.136	0.0021	0.075
0.01	0.84	1.63	0.06	5.6	<3e-2	20	0.007	0.0018	0.15
0.005	0.84	1.25	0.048	27(¿)	2e-3	20	(¿)	0.023	0.315(¿)

Table 2 – Identified structural and physicochemical parameters.

SOC	a_{eNi}/cm^{-1}	a_{eMH}/cm^{-1}	$i^{o}_{MH}a_{aMH}/Acm^{-3}$	$i^{o}_{Ni}a_{aNi}/Acm^{-3}$	$(soc(1-soc)c_m a_a\sqrt{D})_{Ni}/mol.cm^{-2}\ s^{-1}$
0.95	1.68×10^4	1.85×10^5	0.0451	8.98	0.1164×10^{-4}
0.85	0.61×10^4	1.9×10^5	0.0438	17.8	0.1318×10^{-4}
0.72	0.36×10^4	2.0×10^5	0.0460	35.9	0.1742×10^{-4}
0.57	0.47×10^4	1.95×10^5	0.0478	45.3	0.1735×10^{-4}
0.43	0.52×10^4	1.94×10^5	0.0514	36.1	0.151×10^{-4}
0.29	0.62×10^4	1.92×10^5	0.0536	40.8	0.1384×10^{-4}
0.15	0.75×10^4	2.7×10^5	0.062	30.2	0.0975×10^{-4}
0.01	2×10^2	0.54×10^4	0.0207	18.7	0.0254×10^{-4}
0.005	(?)	0.56×10^4	0.0056	1.64	0.0124×10^{-4}(¿)

$$a_e = \frac{C_i}{C_{dl}\lambda_i L A_p};\quad \kappa = \frac{L}{A_p\lambda_i}$$
$$i^{o}a_a = \frac{RT}{\Re_i\lambda_i F V_e};\quad a_a c_m\sqrt{D}soc(1-soc) = \frac{RT}{F^2\Delta_i\lambda_i V_e} \qquad (17)$$

Eqs. (17) may be used to derive identification criteria in order to assign electrode 1 and 2 to either Ni or MH electrodes. For this purpose previously known parameters are used:

Construction parameters:

$L_{Ni} = 0.074$ cm; $A_{pNi} = 0.51$ cm^2
$L_{MH} = 0.17$ cm; $A_{pMH} = 0.8$ cm^2

Parameters from the bibliography for electrodes of analogous materials:

$i^{o}_{1ref}a_{aMH} < 3 \times 10^{-1}$ A.cm^{-3} [18]

$a_{eMH} = 2 \times 10^5$ cm^{-1} [2]

As the Ni electrode controls the battery SOC, i.e. $soc_{Ni} = soc_{BAT}$, other diagnostic criteria are the dependence of

$$i^{o}_{Ni}a_{aNi} = \frac{RT}{\Re_{Ni}\lambda_{Ni}FL_{Ni}A_{pNi}} \text{ with } soc_{BAT}$$

given by

$$i^{o}_{Ni}a_{aNi} = 2i^{o}_{Ni,ref}a_{aNi}\left(\frac{soc_{Ni}^{\alpha_a}}{(1-soc_{Ni})^{(\alpha_a-1)}}\right) = \frac{RT}{\Re_{Ni}\lambda_{Ni}FL_{Ni}A_{pNi}}$$

and the dependence of

$$a_{aNi}c_{mNi}\sqrt{D_{Ni}}soc_{Ni}(1-soc_{Ni}) = \frac{RT}{F^2\Delta_{Ni}\lambda_i L_{Ni}A_{pNi}} \text{ with } soc_{BAT}$$

Based on the diagnostic criteria given above, it was possible to assign electrode "2" to the Ni electrode. Some physicochemical and structural parameters could be determined as depicted in Table 2.

4.2. *Dependence of the kinetic parameters with soc_{BAT}*

The theoretical curve of Fig. 5 was calculated with

$$i^{o}_{Ni}a_{aNi} = 2i^{o}_{Ni,ref}a_{aNi}\left(\frac{SOC_{BAT}{}^{\alpha a}}{(1-soc_{BAT})^{(\alpha_a-1)}}\right)$$

Assuming $i^{o}_{Ni,ref}a_{aNi} = 40$ A.cm^{-3} y $\alpha_a = 0.5$

From Fig. 5, it can be observed that the values of $i^{o}_{1ref}a_{aNi}$ derived from the fitted parameters, assigning electrode "2" to Ni, reproduce relatively well the expected dependence with soc_{BAT}.

The theoretical curve of Fig. 6 was calculated assuming that $a_{aNi}C_{mNi}D_{Ni}^{0.5} = 6.9 \times 10^{-5}$ mol cm^{-2}.s^{-1}

Also Fig. 6 shows the expected dependence of $a_{aNi}c_{mNi}\sqrt{D_{Ni}}soc_{BAT}(1-soc_{BAT})$ with soc_{BAT}, validating the assignation of electrode "2" to Ni.

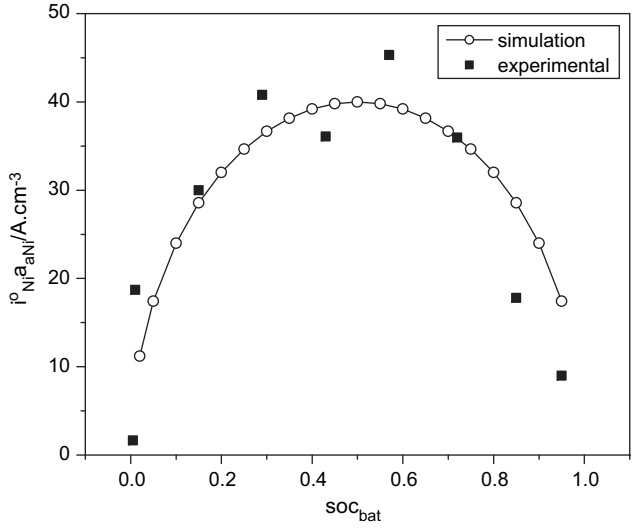

Fig. 5 – Experimental (■) and theoretical (–○–) dependence of $i^{o}_{Ni}a_{aNi}$ with soc_{BAT}.

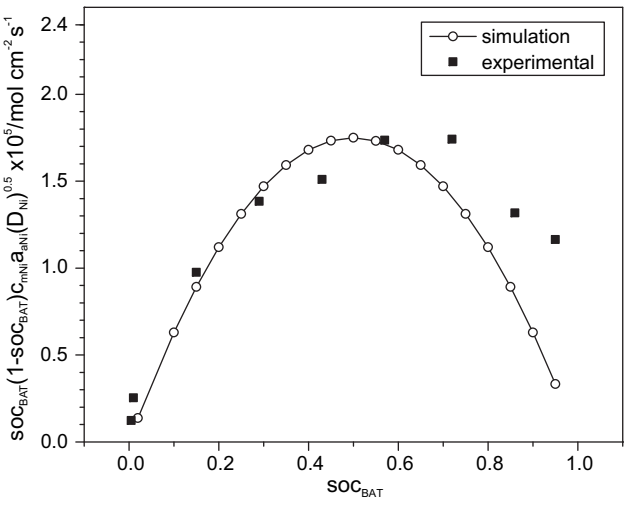

Fig. 6 – Experimental (■) and theoretical (–○–) dependence of $soc_{BAT}(1-soc_{BAT})c_{mNi}a_{aNi}(D_{Ni})^{0.5}$ with soc_{BAT}.

5. Conclusions

- The EIS response of a Ni–MH battery was simulated in terms of a physicochemical model, considering the electrodes as porous flooded structures where the electrochemical processes take place at the active material/electrolyte interface.
- The structural analysis of the model indicates that the Ni and MH electrodes are indistinguishable and the individual kinetic and structural parameters are not identifiable from impedance data, unless previous knowledge of certain parameters is available.
- Diagnostic criteria, based on previously known parameters and on the dependence of kinetic and mass transport parameters with the battery SOC, have been used to distinguish between the Ni and MH electrodes.
- The fulfillment of the expected dependence of the parameters derived from the fitting procedure with soc_{BAT} constitutes a validation of the proposed model and the identification analysis.

Acknowledgements

The authors acknowledge the financial support given by the following Argentina organizations: Consejo Nacional de Investigaciones Científicas y Técnicas, Agencia Nacional de Promoción Científica y Tecnológica, Universidad Nacional de La Plata, Centro Atómico Bariloche and Instituto Balseiro and Universidad Nacional del Comahue.

Nomenclature

A_{pNi}	Geometric area, cross section, of the Ni electrode/cm^2
A_{pMH}	Geometric area, cross section, of the MH electrode/cm^2
a_{eNi}	Total interfacial area per unit volume in the Ni electrode/cm^{-1}
a_{eMH}	Total interfacial area per unit volume in the MH electrode/cm^{-1}
a_{aNi}	Active area per unit volume in the Ni electrode/cm^{-1}
a_{aMH}	Active area per unit volume in the MH electrode/cm^{-1}
$Cdl_{MH} = Cdl_{Ni}$	5E-5/Fcm^{-2}
c_{mNi}	Maximum H concentration in the Ni active material/$mol.cm^{-3}$
c_{mMH}	Maximum H concentration in the MH active material/$mol.cm^{-3}$
D_{Ni}	Diffusion coefficient of H in the Ni electrode/$cm^2\ s^{-1}$
D_{MH}	Diffusion coefficient of H in the MH electrode/$cm^2\ s^{-1}$
i^o_{Ni}, i^o_{MH}	Exchange current densities of Ni and MH electrodes (SOC dependent)/$A.cm^{-2}$
$i^o_{Ni,ref}$, $i^o_{MH,ref}$	Exchange current densities of Ni and MH electrodes at the reference state (SOC = 0.5)
κ_{Ni}	Electrolyte effective conductivity in the Ni electrode/$ohm^{-1}cm^{-1}$
κ_{MH}	Electrolyte effective conductivity in the MH electrode/$ohm^{-1}cm^{-1}$
L_{Ni}	Ni electrode length/cm
L_{MH}	MH electrode length/cm
R_i	Internal resistance of the battery (Z_{BAT} for $f \to$ inf)/ohm
soc_{Ni}	Ni electrode state of charge
soc_{MH}	MH electrode state of charge
soc_{BAT}	Battery state of charge
x_{sNi}	Fractional concentration of hydrogen atoms in the Ni particles at the electrochemical interface.
x_{sMH}	Fractional concentration of hydrogen atoms in the MH particles at the electrochemical interface
x_{refNi}, x_{refMH}	H fractional concentration in the reference state, $x_{ref} = 0.5$
Z_{pNi}	Impedance of Ni electrode per unit geom.area/ohm cm^2
Z_{pMH}	Impedance of MH electrode per unit geom. Area/ohm cm^2
σ_{Ni}	Effective conductivity of the solid phase in the Ni electrode/$ohm^{-1}cm^{-1}$
σ_{MH}	Effective conductivity of the solid phase in the MH electrode/$ohm^{-1}cm^{-1}$

REFERENCES

[1] Bundy K, Karlsson M, Lindbergh G, Lundqvist A. An electrochemical impedance spectroscopy method for prediction of the state of charge of a nickel-metal hydride battery at open circuit and during discharge. J Power Sources 1998;72:118–25.
[2] Castro EB, Real SG, Bonesi A, Visintin A, Triaca WE. Electrochemical impedance characterization of porous metal hydride electrodes. Electrochim Acta 2004;49:3879–90.
[3] Castro BE, Milocco RH. Identifiability of sorption and diffusion processes using EIS: application to the hydrogen reaction. J Electroanal Chem 2005;579:113–23.
[4] Cheng S, Zhang J, Liu H, Leng Y, Yuan A, Cao Ch. Study of early cycling deterioration of a Ni/MH battery by electrochemical impedance spectroscopy. J Power Sources 1998;74:155–7.
[5] Gu WB, Wang CY, Li SM, Geng MM, Liaw BY. Modeling discharge and charge characteristics of nickel–metal hydride batteries. Electrochim Acta 1999;44:4525–41.
[6] Hammouche A, Karden E, de Doncker RW. Monitoring state-of-charge of Ni–MH and Ni–Cd batteries using impedance spectroscopy. J Power Sources 2004;127:105–11.
[7] Huet F. A review of impedance measurements for determination of the state-of-charge or state-of-health of secondary batteries. J Power Sources 1998;70:59–69.
[8] Jacobsen T, West K. Diffusion impedance in planar, cylindrical and spherical symmetry. Electrochim Acta 1995; 40:255–62.
[9] Meyers JP, Doyle M, Darling RM, Newman J, Newman JJ. The impedance response of a porous electrode composed of intercalation particles. J Electrochem Soc 2000;147:2930.
[10] Micka K, Rousar I. Theory of porous electrodes—XVI. The nickel hydroxide electrode. Electrochim Acta 1980;25: 1085–90.
[11] Milocco, RH, Castro, EB. State of charge estimation in Ni–MH rechargeable batteries. J Power Sources 2009;194:558–567.
[12] Nelatury SR, Singh P. Equivalent circuit parameters of nickel/metal hydride batteries from sparse impedance measurements. J Power Sources 2004;132:309–14.
[13] Paxton B, Newman J. Modeling of Nickel/Metal hydride batteries. J Electrochem Soc 1997;144:3818–31.
[14] Real SG, Ortiz M, Castro EB. The discharge process of nickel hydroxide electrodes used in batteries: a dynamic analysis study by EIS. Int J Hydrogen Energy 2008;33:3493–5.

[15] Rodrigues S, Munichandraiah N, Shukla AK. A review of state-of-charge indication of batteries by means of a.c. impedance measurements. J Power Sources 2000;87:12–20.
[16] Thele M, Bohlen O, Sauer DU, Karden E. Development of a voltage-behavior model for NiMH batteries using an impedance-based modeling concept. J Power Sources 2008; 175:635–43.
[17] Verbrugge M, Tate E. Adaptive state of charge algorithm for nickel metal hydride batteries including hysteresis phenomena. J Power Sources 2004;126:236–49.
[18] Visintin A, Castro EB, Real S, Triaca WE, Wang C, Soriaga MP. Electrochemical activation and electrocatalytic enhancement of a hydride-forming metal alloy modified with palladium, platinum and nickel. Electrochim Acta 2006;51:3658–67.